Ambiently and Mechanically Stable Ionogels for Soft Ionotronics

Burebi Yiming, Xiao Guo, Nasir Ali, Nan Zhang, Xinning Zhang, Zilong Han, Yuchen Lu, Ziliang Wu, Xiulin Fan, Zheng Jia,* and Shaoxing Qu

Stretchable ionic conductors such as hydrogels and ionic-liquid-based gels (aka ionogels) have garnered great attention as they enable the development of soft ionotronics. Notably, soft ionotronic devices inevitably operate in humid environments or under mechanical loads. However, many previously reported hydrogels and ionogels, however, are unstable in environments with varying humidity levels owing to hydrophilicity, and their liquid components (i.e., ionic liquid, water) may leak easily from polymer matrices under mechanical loads, causing deterioration of device performance. This work presents novel hydrophobic ionogels with strong ionic liquid retention capability. The ionogels are ambiently and mechanically stable, capable of not absorbing moisture in environments with high relative humidity and almost not losing liquid components during long periods of mechanical loading. Moreover, the ionogels exhibit desirable conductivity (10^{-4}–10^{-5} S cm^{-1}), large rupturing strain (>2000%), moderate fractocohesive length (0.51–1.03 mm), and wide working temperature range (−60 to 200 °C). An ionic skin is further designed by integrating the concept of sensory artificial skins and triboelectric nanogenerators, which can convert multiple stimuli into various types of signals, including resistance, capacitance, short-circuit current, and open-circuit voltage. This work may open new avenues for the development of soft ionotronics with stable performance.

1. Introduction

Stretchable conductive materials have enabled the development of flexible electronics, such as field effective transistor arrays,[1] devices for human motion detection,[2] skin-like sensors,[3] energy harvesting devices,[4] and stretchable batteries.[5,6]

In general, conductive materials can be categorized into two types, namely, electronic conductors and ionic conductors. Metals, the most commonly used electronic conductors, are usually rigid and nonstretchable—incompatible with the requirement of soft machines and wearable devices. Structural design strategies using serpentine patterns,[7,8] kirigami-inspired structures,[9,10] and thin-film conductors with patterned microcracks[11,12] can endow metal materials with much-enhanced stretchability. Depositing metal thin films on wrinkled or prestrained substrates[4,13–15] is another strategy for the fabrication of stretchable metal conductors. However, engineering stretchable metal conductors often require multistep, costly, and material-specific fabrication processes, and the fabricated stretchable structures suffer from limitations such as nontransparency and delamination of metal layers from underlying substrates.[15,16] 1D or 2D electrically conducting materials such as carbon nanotubes (CNTs), graphene, and silver nanowires (AgNWs) are widely used to achieve stretchable transparent conductors recently. Coating a thin layer of CNTs, graphene, and AgNWs on a wrinkled compliant substrate as well as embedding these conducting materials in an insulating elastomeric matrix as a percolated conductive filler network is also a major route toward stretchable electrical conductors.[17–19] Nevertheless, the out-of-plane patterns of the wrinkled composite

B. R. B. Yiming, Z. L. Han, Y. C. Lu, Prof. Z. Jia, Prof. S. X. Qu
Key Laboratory of Soft Machines and Smart Devices of
Zhejiang Province
Center for X-Mechanics
Department of Engineering Mechanics
Zhejiang University
Hangzhou 310027, China
E-mail: zheng.jia@zju.edu.cn
X. Guo
Department of Mechanical Engineering
National University of Singapore
Singapore 117575, Singapore

The ORCID identification number(s) for the author(s) of this article can be found under https://doi.org/10.1002/adfm.202102773.

N. Ali
Department of Physics
State Key Laboratory of Silicon Materials
Zhejiang University
Hangzhou 310027, China
N. Zhang, Prof. X. L. Fan
State Key Laboratory of Silicon Materials
School of Materials Science and Engineering
Zhejiang University
Hangzhou 310027, China
X. N. Zhang, Prof. Z. L. Wu
Ministry of Education Key Laboratory of Macromolecular Synthesis
and Functionalization
Department of Polymer Science and Engineering
Zhejiang University
Hangzhou 310027, China

ADVANCED
SCIENCE NEWS
www.advancedsciencenews.com

ADVANCED
FUNCTIONAL
MATERIALS
www.afm-journal.de

structures and the damage of the percolation network during cyclic loading could be disadvantageous for devices that require planar interfaces and cycling stability. Conducting polymers, which rely on the transport of electrons to conduct electricity,[20] are another kind of electronic conductors. One of these polymers is poly(3,4-ethylenedioxythiophene):polystyrene sulfonate (PEDOT:PSS), which has attracted considerable attention in the field of stretchable electronics owing to its high conductivity. However, many conducting polymers often exhibit low transmittance and limited stretchability (≈5% for PEDOT:PSS).[1] Developing stretchable and transparent conducting polymers with stretchability beyond 1000% remains challenging.

Inspired by biological tissues, in which electricity is transferred through the movement of ions, stretchable ionotronics has emerged.[21–24] With the advent of soft ionotronic devices, intrinsically stretchable ionic conductors are urgently needed. Hydrogels have been considered as ideal ionic conductors: They are stretchable and transparent, with desirable ionic conductivity, thereby enabling ionotronic devices such as ionic skins,[25–28] artificial muscles,[29] and energy harvesting devices.[30,31] However, a common problem of hydrogel-based conductors is that the operating temperature of hydrogels is limited to room temperature—the material freezes at subzero temperatures and rapidly loses water when exposed to open air. Introducing salts into hydrogels can enhance their water retention capability[32,33] but cannot fully prevent dehydration, especially at high temperatures. Moreover, hydrogels do not adhere well to other materials.[23] Organogels and organohydrogels have also been used as ionic conductors for developing soft ionotronic devices.[34–36] For example, a biomimetic ionic spider web with excellent capturing and self-cleaning capabilities has been demonstrated based on ion-conducting organogel that contains organic solvent dissolving lithium salts.[37] Notably, for some organogels and organohydrogels, encapsulation and plasma etching treatment of the encapsulation layer are required to prevent the evaporation and leakage of liquid solvents. To overcome limitations of hydrogels and organogels inherent to the liquid phase, all-solid-state ionic conductive materials, such as ionic conducting elastomers (ICEs), ionoelastomers, and polymeric-ionic-liquid (IL)-based elastomeric conductors, have emerged recently.[38–41] Nevertheless, these materials usually possess relatively low ionic conductivity and may absorb moisture in humid environments owing to their hygroscopic nature.[40]

Ionic-liquid-based gels (aka ionogels) have attracted considerable attention for their applications as ionic conductors in soft ionotronics[42,43] owing to their excellent thermal stability, high ionic conductivity, and wide electrochemical window. Ionogels are superior to hydrogels in terms of thermal stability—They are not prone to evaporation so that they can be used in open environments without encapsulation.[44] Compared with liquid-free ionic conductors, such as ICEs and ionoelastomers,[40,41] ionogels often possess higher ionic conductivity and are transparent. In practical applications, soft ionotronic devices often operate in humid environments, and thus ideal ionogels for soft ionotronics must be stable in environments with varying humidity levels. However, many ionogels absorb water from the open air owing to the hygroscopic nature of the IL used,[44–46] and some ionogels even undergo hydrolysis in humid environments,[47,48]
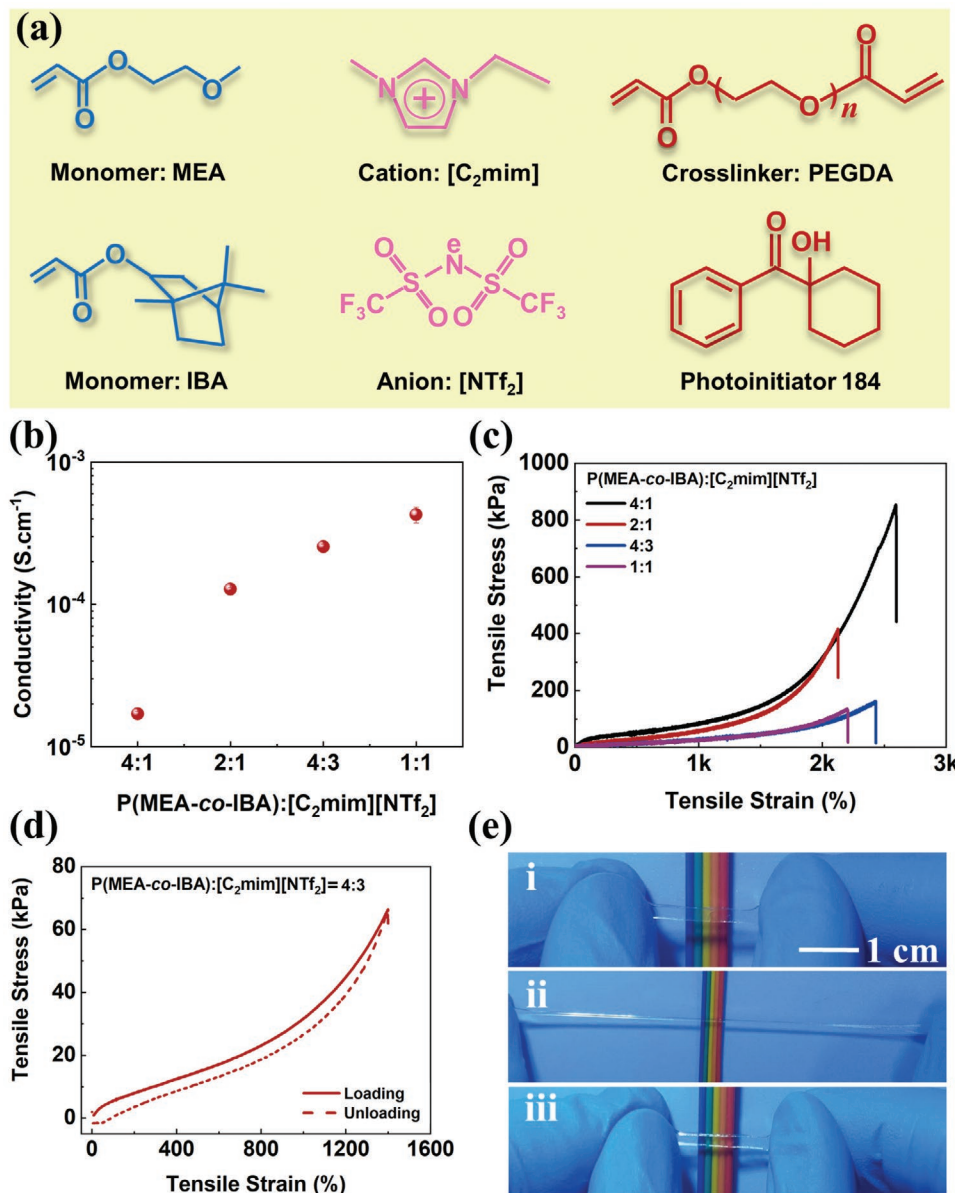
rendering these ionogels not ambient-stable. In addition, soft ionotronic devices such as ionic skins for pressure sensation inevitably work under mechanical loads. Nevertheless, many ionogels suffer from leakage of ILs when being compressed,[49] such that they are not mechanical-stable. Thus far, many previously reported ionogels possess either mechanical stability or ambient stability. But ionogels that are both ambient-stable and mechanical-stable have rarely been reported.

In this work, to fabricate ambiently and mechanically stable ionogels, we use an ultrastretchable single-network copolymer as the polymer matrix, and select a hydrophobic IL with low viscosity—which contributes to the hydrophobicity and low hysteresis of the fabricated ionogels—as the conductive liquid phase. The ionogel reported here is ultrastretchable, having a fracture strain exceeding 2000%, a wide working temperature range of −60 to 250 °C, a broad electrochemical window exceeding 3.5 V, and strong adhesion to dielectric elastomers, rendering the material an ideal candidate for soft ionotronic devices. Most importantly, the ionogels are stable in humid environments with varying humidity levels and almost do not suffer from liquid leakage even when subject to mechanical loads for a relatively long period. Besides, fractocohesive length—the characteristic flaw size below which a material becomes flaw-insensitive—of the ionogels in this work is in the range of 0.51–1.03 mm. To the best of our knowledge, this is the first time that the fractocohesive length for ionogels is reported. To demonstrate the application of the ionogel for soft ionotronics, we develop a novel multimodal ionic skin—by integrating the concept of sensory ionic skins and triboelectric nanogenerators (TENGs)—that can convert a variety of external stimuli, such as pressure, stretch, and temperature, into four types of electrical signals, including resistance, capacitance, open-circuit voltage (OCV), and short-circuit current (SCC). The self-generated OCV can reach several volts, which is orders of magnitude higher than that generated by conventional sensory ionic skins, endowing the ionic skin with energy harvesting and self-charging capabilities.

2. Results and Discussion

2.1. Preparation of the Ionogels

We use the IL 1-ethyl-3-methylimidazolium bis(trifluoromethylsulfonyl)imide ([C$_2$mim][NTf$_2$]) as the ionic conductive phase because of its hydrophobicity, high ionic conductivity, and low viscosity.[50] The copolymer of acrylate monomers, i.e., ethylene glycol methyl ether acrylate (MEA) and isobornyl acrylate (IBA), is used as the polymer network. The molar fraction of IBA monomer in the copolymer is denoted by $F = M_{IBA}/(M_{MEA} + M_{IBA})$. The copolymer P(MEA-co-IBA) of $F = 0.3$ is used in this work owing to its better mechanical properties compared to copolymers with other compositions.[51] We fabricate the ionogels using a facile photocuring process. Appropriate amounts of acrylate monomers (i.e., MEA and IBA) are mixed with the IL [C$_2$mim][NTf$_2$]. Polyethylene glycol diacrylate (PEGDA) and 1-hydroxycyclohexyl phenyl ketone (photoinitiator 184) are added as the cross-linker and photoinitiator, respectively (All chemicals used are shown in **Figure 1**a).

ADVANCED
SCIENCE NEWS
www.advancedsciencenews.com

ADVANCED
FUNCTIONAL
MATERIALS
www.afm-journal.de

Figure 1. Synthesis and physical properties of the ionogels. a) Molecular structures of MEA and IBA monomers, cations and anions of the IL, cross-linker PEGDA, and photoinitiator 184. b) Conductivity of ionogels with different IL contents. c) Stress–strain curves of ionogels with different IL contents. All samples have stretchability exceeding 2000%. d) The loading–unloading curve of the ionogel with an IL content of 4:3. e) Photographs of an ionogel sample with a 4:3 IL content: (i) initial, (ii) stretched, and (iii) recovered state. After being stretched to ≈9 times its original length, the sample almost recovers its original length immediately, demonstrating fast self-recovery behavior (Scale bar: 1 cm).

The weight percentage of the cross-linker and photoinitiator relative to the total amount of copolymer and IL are fixed at 0.2 and 1 wt%. Four representative ionogels, which are denoted as P (MEA-*co*-IBA): [C$_2$mim][NTf$_2$] = 4:1, 2:1, 4:3, and 1:1 (volume ratio) according to the IL content, are fabricated for testing.

2.2. Basic Properties of the Ionogels

Ionic conductivity of the ionogels is calculated by $\sigma = L/(AR)$, where L is the sample length, A the cross-sectional area of the sample, and R the bulk resistance. The ionic conductivity

of the ionogels varies from 1.69×10^{-5} to 4.27×10^{-4} S cm^{-1} (Figure 1b). All ionogels exhibit high stretchability, with elongation at break exceeding 2000% (Figure 1c). The ionogel with a 4:1 IL content has the highest stretchability of ≈2580% (Figures S1 and S2, Supporting Information). The reversibility of the ionogels is investigated by loading–unloading tests. The samples are loaded to a strain of 1400% at a loading rate of 100 mm min^{-1}. The loading–unloading curve of the sample with an IL content of 4:3 shows a highly reversible mechanical response with little hysteresis (Figure 1d). The hysteresis of the ionogels decreases with increasing IL content (Figure S3, Supporting Information), largely because of the low viscosity of

the IL. Figure 1e shows a sample with an IL content of 4:3 can immediately recover its original length after being stretched to ≈9 times its original length. The ionogels with an IL content of 4:3 have a residual strain of ≈100% after ten consecutive stretching–releasing cycles with the applied strain up to 1000%, achieving a recovery ratio of ≈90% (Figure S4, Supporting Information).

2.3. Stability of the Ionogels

We investigate the stability of the ionogels at elevated/low temperatures, in environments with high relative humidity (RH), and under mechanical loads. To explore the high-temperature tolerance of the ionogels, the thermal decomposition temperature of the ionogels is determined by the thermal gravimetric analysis (TGA) in air and nitrogen environment. The ionogels exhibit a high decomposition temperature of ≈200 °C (**Figure 2**a) in air and ≈250 °C in the nitrogen environment (Figure S5, Supporting Information), above which the decomposition of ionic liquid and thermal degradation of the polymer network—such as depolymerization, random chain scission, and side-group elimination—may take place. In stark contrast, pure polyacrylamide (PAAm) hydrogels and salt-containing PAAm hydrogels lost ≈80% of their weights before the temperature reaches 100 °C (Figure 2a). We further compare the thermal stability of the ionogels and PAAm hydrogel containing 8 M LiCl by measuring the weight of the samples
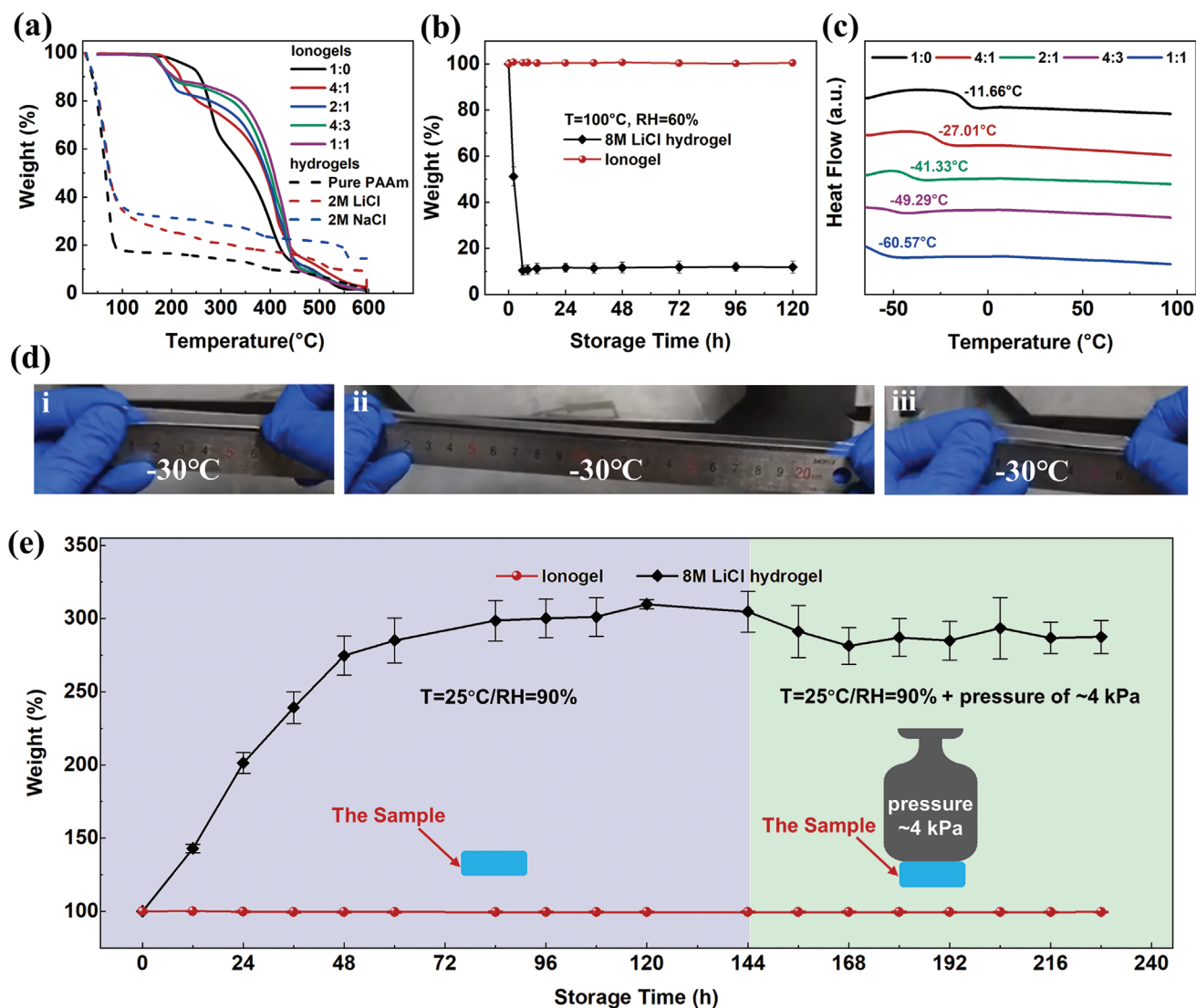
Figure 2. Stability of the ionogels. a) The TGA results of the ionogels with different IL contents, which demonstrates a high decomposition temperature of the ionogels exceeding 200 °C in air. b) High-temperature tolerance of the ionogels. c) The DSC curves of the ionogels with different IL contents. The glass transition temperature decreases from −11.66 to −60.57 °C as the IL content increases from 1:0 to 1:1. d) An ionogel sample of IL content of 4:3 remains elastic and stretchable at −30 °C, (i) original length, (ii) stretched up to ≈4 times its original length, (iii) quickly return to the original length after the stretch is released. e) Ambient and mechanical stability of the ionogels. An ionogel sample (with an IL content of 4:3) well maintains its weight at a relative humidity of 90%, even when it is compressed by a stress of ≈4 kPa.

**ADVANCED
SCIENCE NEWS**
www.advancedsciencenews.com
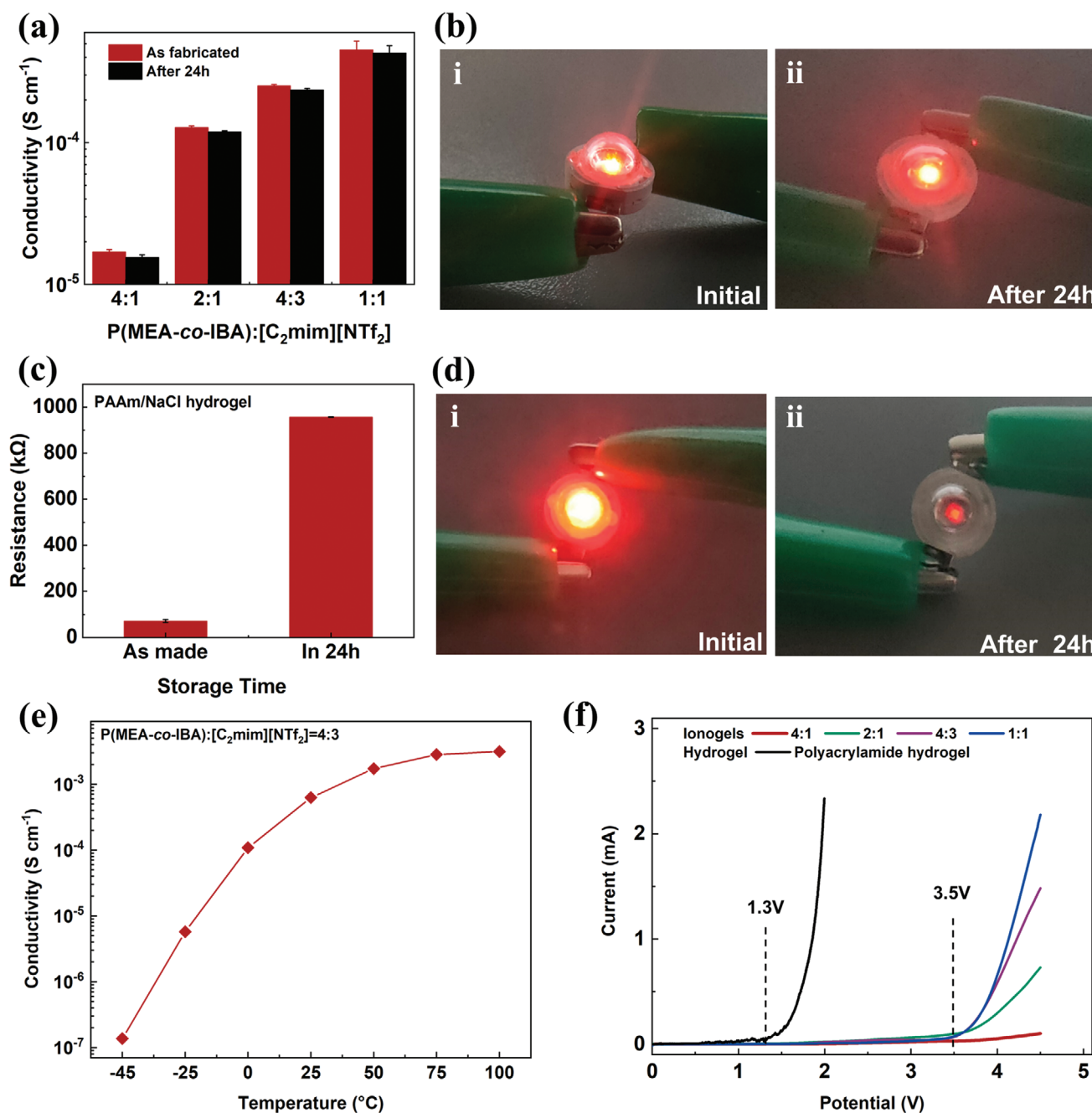
**ADVANCED
FUNCTIONAL
MATERIALS**
www.afm-journal.de

placed in a thermostatic humidity chamber with the temperature and RH fixed at 100 °C and 60%, respectively. The ionogel samples exhibit negligible weight change during the whole testing period. By contrast, owing to water evaporation, the PAAm hydrogel containing 8 M LiCl loses 50% of its weight within 2 h and 90% of its weight after 6 h of testing (Figure 2b). Similarly, it has been reported that the organogel consisting of PAAm networks and ethylene glycol (EG) dissolving lithium chloride (LiCl) loses ≈10% of its initial weight after 20 h under harsh conditions.[37] The ionogels reported here demonstrate good thermal stability and thus can be used in the open air even at high temperatures.

To explore the low-temperature tolerance of the ionogels, we perform differential scanning calorimetry (DSC) to measure the glass transition temperature (T_g) of the material, above which the ionogels remain stretchable and conductive. Five representative samples are tested, including the pure P (MEA-co-IBA) sample (with an IL content of 1:0) and four ionogel samples with different IL contents. The ionogel is composed of the copolymer backbone and IL, thus T_g of ionogels is determined by that of both components. The pure copolymer has a T_g of −11.66 °C and the T_g of IL is −96.6 °C.[50] Therefore, T_g of the ionogels decreases with increasing IL content (Figure 2c). An ionogel sample of a 4:3 IL content has a T_g of −49.29 °C, and thus it can maintain its elasticity and stretchability at −30 °C: The sample that is stretched to ≈4 times its original length can recover its original length immediately after the strain is released (Figure 2d). Different from hydrogels which freeze at subzero temperatures and evaporate at ambient conditions, the extreme temperature tolerance of the ionogels endows them with antifreezing capability at low temperatures (as low as −60 °C for the 1:1 IL content) and nonvolatility at high temperatures (up to ≈200 °C).

We next study the ambient and mechanical stability of the ionogels. Ionogel samples of a 4:3 IL content and PAAm hydrogel samples containing 8 M LiCl are kept in a thermostatic humidity chamber of 90% RH and 25 °C. Negligible change in the weight of the ionogel samples is observed within 144 h of the testing period, whereas the weight of the hydrogels increases by 40% within 12 h and by ≈200% in the next 60 h owing to continuous absorption of moisture (Figure 2e). Notably, many previously reported ionogels are unstable when subject to humidity change as the hygroscopic nature of the selected IL leads to moisture absorption.[44,46] For example, the PAA/IL ionogel—which consists of poly(acrylic acid) (PAA) and 1-ethyl-3-methylimidazolium ethyl sulfate (the ionic liquid)— shows remarkable weight change as the RH varies.[52] To confirm the hydrophobicity of the ionogels reported in this work— i.e., the mechanism underpinning the ambient stability of the ionogels, we perform the contact angle (CA) tests of the pure copolymer matrix and the ionogels containing different IL contents (Figure S6, Supporting Information). The pure copolymer matrix has a CA of ≈105°, showing excellent hydrophobicity. The ionogels exhibit even larger CA than the copolymer matrix does, and the CA increases with increasing IL content. The ionogels with an IL content of 1:1 possess the largest CA of ≈121°. The highly hydrophobic nature of the copolymer matrix and IL contributes to the excellent ambient stability of the ionogels. In addition to ambient stability, mechanical stability is also critical to the performance of ionogel-based ionotronic

devices, as such devices inevitably operate under mechanical loadings. Herein, we monitor the weight change of the ionogels (with a 4:3 IL content) under a compressive stress of ≈4 kPa at a high RH of 90%. The ionogels show negligible changes in their weights after 72 h of testing (Figure 2e), demonstrating the strong capability of ionic liquid retention under mechanical compression. In contrast, the 8 M LiCl-containing hydrogel samples lose 10–30% of their original weights under the same condition, owing to the leakage of water under mechanical loads. Also, it has been reported that when the PAA/IL ionogel is squeezed against a plain paper, the ionic liquid leaks on the paper under mechanical loads, which is a sign of liquid loss under mechanical loading.[49] It is believed that the hydrogen bonds formed between the copolymer network and IL in our ionogels lock the IL in the copolymer matrix,[50] thereby imparting good mechanical stability to the ionogels. Herein, we would like to mention that although the ionogel reported in this work does not easily lose liquid components upon mechanical loadings, the liquid may leak under some particular conditions such as immersion in miscible solvents. Moreover, the ionic liquid may cause safety and corrosion issues when the ionogels are in direct contact with human skin and some metals. In this sense, encapsulation might still be necessary for related applications.

Additionally, the ionogels exhibit stable electrical performance, as exemplified by stable conductivity over time, conductivity in a wide range of temperatures, and a wide electrochemical window. We measure the conductivity of the as-fabricated ionogels and ionogels stored in ambient conditions for 24 h. It is found that the ionogels maintain 98% of their initial conductivity values after 24 h storage in ambient conditions (**Figure 3**a). It has been reported that some other ionogels such as the PAA/IL ionogel loses ≈30% of its initial conductivity at ambient conditions in 24 hours.[49] To visually illustrate the stable conductivity, we power up a light-emitting diode (LED) with a conductive wire made from the ionogel samples (Figure 3b (i)). Negligible change in LED light intensity is observed after 24 h (Figure 3b (ii)). In sharp contrast, after being exposed to the open air for 24 h, a 2 M NaCl-containing PAAm hydrogel sample almost loses its conductivity, with the resistivity increases by more than tenfolds (Figure 3c), and fails to light an LED (Figure 3d), demonstrating poor electrical stability. Moreover, the ionogels are conductive for a wide range of temperatures. We measure the bulk resistance of ionogel samples (of a 4:3 IL content) by using the Nyquist plots (Figure S7, Supporting Information) and evaluate the conductivity of the ionogels at different temperatures. The conductivity of the ionogels increases from 1.38×10^{-7} at −45 °C to 3.14×10^{-3} S cm^{-1} at 100 °C (Figure 3e). This can be attributed to the fact that elevated temperature leads to more intense movement of copolymer chains and ions and thus results in higher conductivities. Also, the linear sweep voltammetry testing indicates that the measured current of a 2 M NaCl-containing PAAm hydrogel increases steeply as the applied voltage exceeds ≈1.3 V, indicating the decomposition of water by electrolysis. In contrast, the ionogel remains stable with negligible current until the applied voltage reaches ≈3.5 V (Figure 3f), largely owing to the high decomposition voltage of the ionic liquid [C$_2$mim][NTf$_2$]. That is, the ionogels have a wider electrochemical window than hydrogel electrolytes do.

**ADVANCED
SCIENCE NEWS**
www.advancedsciencenews.com
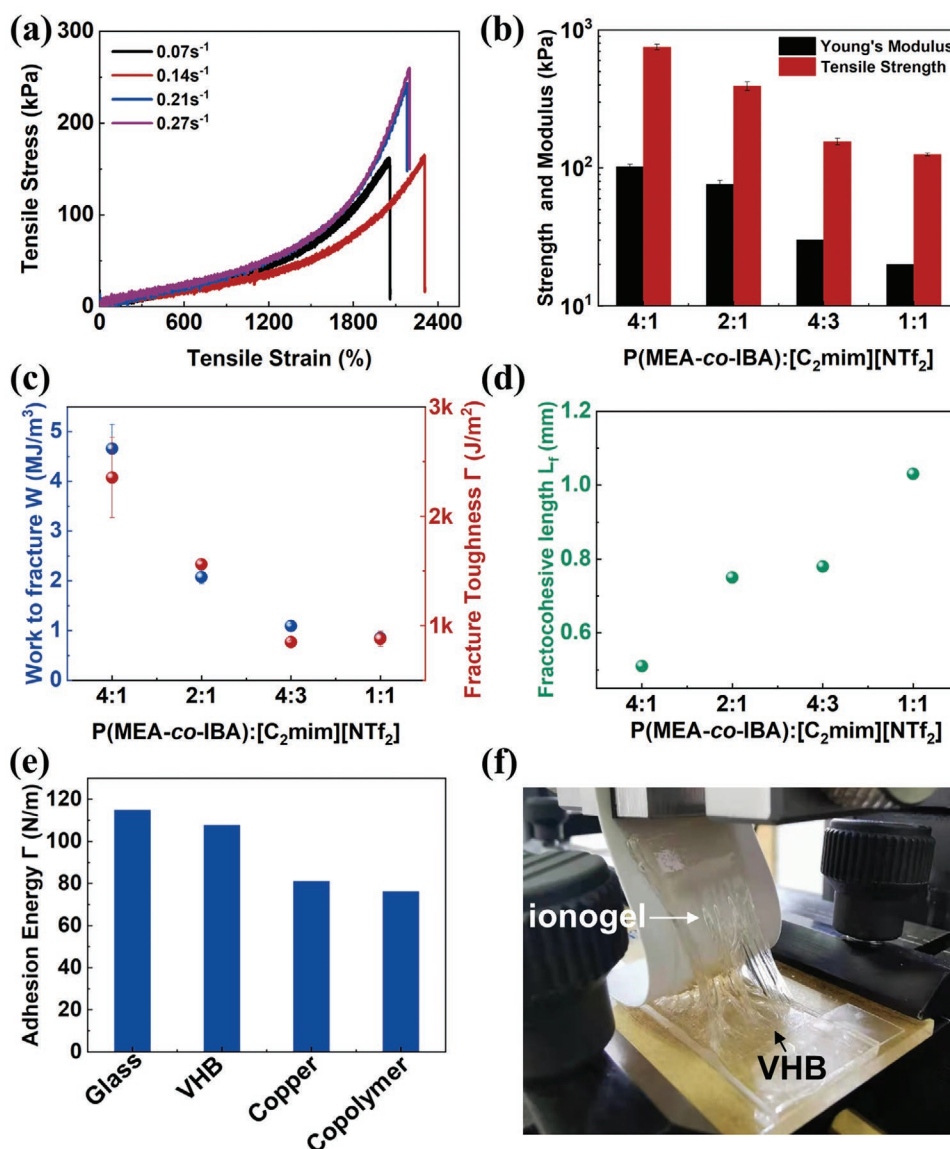
**ADVANCED
FUNCTIONAL
MATERIALS**
www.afm-journal.de

Figure 3. Stable electrical performance of the ionogels. a) Conductivity of the as-fabricated ionogels versus conductivity of ionogels stored in ambient conditions for 24 h. b) (i) An LED powered by the as-made ionogel wire; (ii) The LED maintains almost the same light intensity after 24 h. c) The PAAm hydrogel containing 2 M NaCl almost loses its conductivity after 24 h storage in ambient conditions owing to dehydration. d) (i) An LED powered by the as-fabricated NaCl-containing PAAm hydrogel; (ii) The LED light becomes dimmed after 24 h owing to the loss of conductivity of the hydrogel. e) The temperature-dependent ionic conductivity of the samples with an IL content of 4:3. The ionogels are conductive in a wide range of temperatures. f) Linear sweep voltammetry testing results of the ionogels and hydrogel electrolytes containing 2 M NaCl.

2.4. Mechanical Properties of the Ionogels

The stress–strain curves of ionogel samples of a 4:3 IL content are measured at different strain rates, which reveals that the ionogel achieves ultrahigh elongation at break beyond 2000% at strain rates ranging from 0.07 to 0.27 s^{-1} (**Figure 4**a). Young's modulus and tensile strength of the ionogels are extracted from

uniaxial stress–strain curves (Figure S1, Supporting Information). Young's modulus of the ionogels decreases from 102 kPa for IL content of 4:1 to 20 kPa for IL content of 1:1, and the tensile strength simultaneously reduces from 752 to 125 kPa. That is, increasing the IL content leads to a reduction in the mechanical properties of ionogels (Figure 4b). It is well known that mechanical properties—such as stretchability, strength, and

**ADVANCED
SCIENCE NEWS**

www.advancedsciencenews.com

**ADVANCED
FUNCTIONAL
MATERIALS**

www.afm-journal.de

Figure 4. Mechanical properties of ionogels. a) Stress–strain curves of ionogel with an IL content of 4:3 at different strain rates. b) Young's modulus and tensile strength of the ionogels of different IL contents. c) Fracture behaviors of the ionogels: work of fracture and fracture toughness are determined by rupturing samples with no cuts and by rupturing samples with large cuts, respectively. d) Fractocohesive length of ionogels versus IL content. e) Adhesion energy of the ionogels to various materials including glass, VHB, copper, and the copolymer of P(MEA-*co*-IBA). f) Photographs demonstrating good adhesion of the ionogel to VHB during the peeling test.

work of fracture—of gels and elastomers are usually flaw-sensitive: a large-size flaw can significantly reduce the ultimate properties of soft material samples. Notably, the ultimate properties of the materials are negligibly affected by a cut shorter than a certain length. This length, which is defined as the fractocohesive length, is the ratio of the fracture toughness to the work of fracture.[53] Though the fractocohesive length of hydrogels and elastomers has been investigated thoroughly,[53,54] such feature of ionogels has rarely been studied. To determine the fractocohesive length of ionogels, we measure the fracture toughness by rupturing samples of long pre-cuts and the work of fracture by rupturing samples of no pre-cuts. The measured fracture toughness of ionogels varies between 880 and 2350 J m^{-2}, and the work of fracture ranges from 0.85 to 4.65 MJ m^{-3} (Figure 4c).

The fractocohesive length of the ionogels increases from 0.51 to 1.03 mm as the IL content increases (Figure 4d), because the average mesh size of ionogels increases with increasing IL content. That is, the stretchability, strength, and work of fracture of the ionogels are insensitive to small cuts below these values.

Soft ionotronic devices often consist of various materials including ionic conductors, dielectric elastomers, and metals, such that strong interfaces between ionic conductors and other materials are preferred for soft ionotronics design. To quantitatively demonstrate the strong adhesion of ionogels to various materials, we perform the 90° peeling test to determine the adhesion energy of ionogel adhered to representative substrates including glass, VHB, copper, and the copolymer of P(MEA-*co*-IBA), the measured adhesion energy is 114.9, 107.7, 81.1, and

76.1 N m^{-1}, respectively (Figure 4e). To put these numbers into context, we compare the results with other adhesive systems: For instance, the natural adhesion between acrylic elastomer and PAAm hydrogel is of adhesion energy about 0.5 N m^{-1}.[55] Silane-modified hydrogels can adhere to PDMS elastomer via covalent bonding, the adhesion energy is 70–100 N m^{-1}.[56] The noncovalent adhesion between PAAm and poly(acrylic acid) hydrogels has an adhesion energy of 75–200 N m^{-1}.[57] The adhesion energy between two pieces of PAAm hydrogel stitched via topological adhesion is 50–150 N m^{-1}.[58] The adhesion energy of PAAm hydrogels adhered to diverse materials including glass, mica, PDMS, skin, and liver using topological adhesion technique reaches 200–400 N m^{-1}.[59] That is, our material is adhesive with adhesion energy comparable to above-mentioned adhesive systems. Experimental photos further demonstrate that the ionogels exhibit tough adhesion interfaces with representative materials such as VHB (Figure 4f) and glass (Figure S8, Supporting Information). The strong adhesion of the ionogels to other materials is further demonstrated by making a steel-ionogel-VHB-ionogel-copper string, of which the ionogel–VHB junctions and ionogel–metal junctions do not delaminate even at a stretch up to 5 (i.e., $\lambda = 5$) (Figure S8, Supporting Information). Notably, the ionogels adhere to various materials via noncovalent bonding such as van der Waals force and hydrogen bonds, just like adhesive tapes do. Hence, the adhesion is tough and instant. The adhesive property of ionogels makes them an ideal candidate for soft ionotronics.

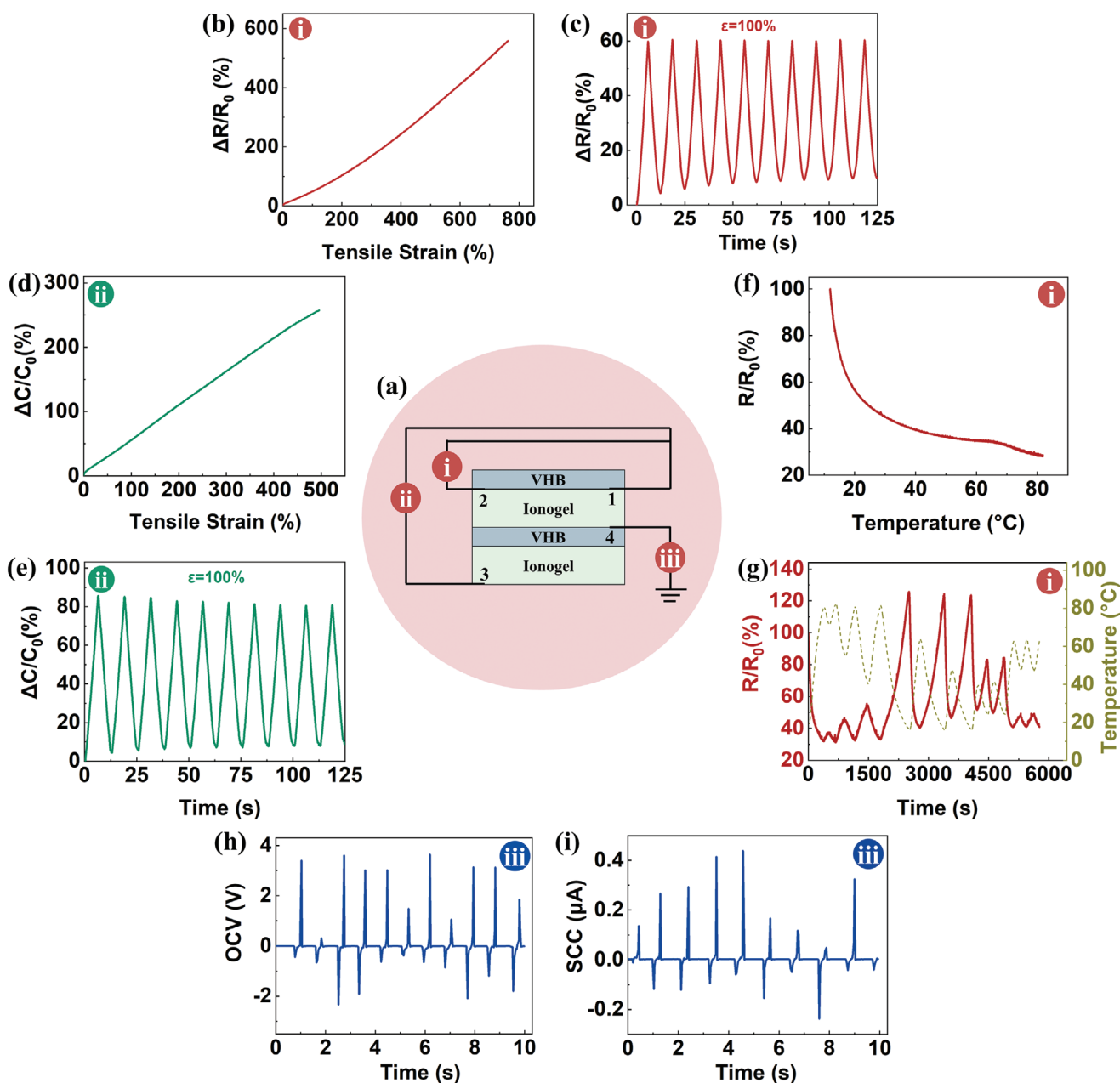### 2.5. A Novel Ionic Skin with Multimodal Sensation

The human skin can sense various environmental stimuli including temperature, deformation, and stress, by harnessing a series of sensory units such as thermoreceptors, mechanoreceptors, and pain receptors.[60] Engineered biomimetic skins that emulate the properties and functions of the human skin may open new avenues toward next-generation wearable electronics and soft robots.[61–63] In this work, to replicate the multimodal sensation capabilities of the human skin, we develop a novel ionic skin, utilizing the ionogel reported above as the ionic conductors. The artificial ionic skin introduced here integrates the concept of TENG and capacitive ionic skin, thus it can convert various mechanical stimuli and temperature into four types of electrical signals, namely, resistance, capacitance, OCV, and SCC. OCV and SCC are self-generated, without external power supplies. As illustrated in **Figure 5**a, the ionic skin contains alternating layers of ionogels and dielectric elastomers: a stack consisting of a thin layer of dielectric elastomer (i.e., VHB) sandwiched between two layers of ionogel samples, which forms a parallel plate capacitor, is covered by another layer of dielectric elastomer. In this system, the resistance change (mode i) can be read from electrodes 1 and 2, the capacitance change (mode ii) can be measured by connecting electrodes 1 and 3, and the self-generated OCV and SCC (mode iii) can be recorded by electrode 4.

When the ionic skin is stretched, the measured resistance and capacitance values increase, enabling the ionic skin to sense the deformation (Figure 5b,d). The ionic skin also demonstrates stable performances under cyclic loadings (Figure 5c,e). The signal drift can be attributed to the viscoelastic behavior of the ionogel and dielectric elastomer. After 200 successive loading–unloading cycles with a maximum tensile strain of 100%, the ionic skin maintains its functionality, demonstrating excellent stability and durability (Figures S9 and S10, Supporting Information). In addition to stretches, the ionic skin can detect pressure by capacitance change. When pressed, the effective area of the capacitor increases, inducing an increase in capacitance, thereby imparting pressure-sensing capability to the ionic skin (Figure S11, Supporting Information). Moreover, the ionic skin can convert temperature changes into resistance signals, as increased temperature enhances ion movement and thus reduces the resistance (Figure 5f). The ionic skin can detect a wide range of temperature variations. The resistance fluctuates between 40% and 120% of the original resistance value when the temperature varies between 15 and 80 °C, and the resistance cycles between 40% and 50% of the original resistance when the temperature varies between 55 and 65 °C (Figure 5g). The ionic skin can convert touch motions into OCV and SCC signals simultaneously. The underlying mechanism is the same as that of the well-known TENG (Figure S12, Supporting Information). When touched by fingers, the ionic skin generates a peak SCC of ≈0.4 µA and a peak OCV of ≈4 V (Figure 5h,i). The generated OCV and SCC increase as the applied loading increases (Figure S13, Supporting Information). Under a given cyclic loading, the OCV and SCC outputs are stable over hundreds of cycles (Figure S14, Supporting Information). Notably, the self-generated OCV is on the order of several volts, much superior to the voltage generated by sensory artificial skins reported before,[28,49] and thus endow the novel ionic skin with energy harvesting and self-charging capabilities.

3. Conclusion

We synthesize a novel ionogel that is both ambiently and mechanically stable, by using a highly stretchable copolymer network, P(MEA-*co*-IBA), and a hydrophobic IL, [C$_2$mim][NTf$_2$]. The designed ionogels do not absorb moisture in humid environments with changing humidity, thanks to the hydrophobicity of the copolymer matrix and the IL, and almost do not suffer from IL leakage even when mechanical loads are exerted for a relatively long time, largely owing to hydrogen bonds formed between the ions and polymer chains which lock the IL in the copolymer matrix. In this sense, the general design principles can be summarized as follows: 1) Using long-chain elastomer networks and hydrophobic ionic liquids to impart good mechanical properties and ambient stability to the ionogels. 2) Taking advantage of molecular interactions (e.g., hydrogen bonds) between elastomer networks and ionic liquids to lock the liquid components in the elastomer matrix, endowing the ionogel with mechanical stability. We believe that the design principles revealed here can be generalized to other material systems for designing ionogels that are both ambient-stable and mechanical-stable. Moreover, we investigate the flaw insensitivity of IL-based gels for the first time: as the average mesh size of ionogels increases with increasing IL contents, the fractocohesive length of the ionogels increases from 0.51 to 1.03 mm. Such values are comparable to that

Figure 5. A novel ionic skin with multimodal sensation capabilities. a) Schematics of the ionic skin design. The circuits highlighted by (i), (ii), and (iii) are linked to three different working modes of the ionic skin, which converts environmental stimuli into signals of resistance, capacitance, and OCV/SCC, respectively. b) Resistance change versus tensile strain. c) Resistance change under cyclic tensile strains between 0% and 100%. d) Capacitance change versus tensile strain. e) Capacitance change under cyclic tensile strains between 0% and 100%. f) Resistance change versus temperature. g) Resistance change in response to temperature fluctuations. h) The OCV curve when the ionic skin is subjected to intermittent touch motions by fingers. i) The SCC curve in response to intermittent touch motions.

reported for elastomers and hydrogels.[53,54] We further develop a novel ionic skin by using the ionogels, which integrates TENGs with capacitive ionic skins and thus can sense a variety of stimuli—including stretch, pressure, and temperature—by converting them into signals of resistance, capacitance, OCV, and SCC. The OCV and SCC signals are self-generated, imparting energy harvesting capability to the ionic skin. The ionogels reported in this work may lead to the development of soft ionotronics and wearable devices with stable performance.

Supporting Information

Supporting Information is available from the Wiley Online Library or from the author.

Acknowledgements

[1] Y. Wang, C. Zhu, R. Pfattner, H. Yan, L. Jin, S. Chen, F. Molina-Lopez, F. Lissel, J. Liu, N. Rabiah, Z. Chen, J. W. Chung, C. Linder, M. F. Toney, B. Murmann, Z. Bao, *Sci. Adv.* **2017**, *3*, 1602076.

[2] Q. Wang, H. Ding, X. Hu, Q. Liu, Z. Li, G. Sun, *Mater. Horiz.* **2020**, *7*, 2673.

[3] J. Kang, D. Son, G.-J. N. Wang, Y. Liu, J. Lopez, Y. Kim, J. Y. Oh, T. Katsumata, J. Mun, Y. Lee, L. Jin, J. B. H. Tok, Z. Bao, *Adv. Mater.* **2018**, *30*, 1706846.

[4] S. Lee, Y. Song, Y. Ko, Y. Ko, J. Ko, C. H. Kwon, J. Huh, S.-W. Kim, B. Yeom, J. Cho, *Adv. Mater.* **2020**, *32*, 1906460.

[5] Z. Song, T. Ma, R. Tang, Q. Cheng, X. Wang, D. Krishnaraju, R. Panat, C. K. Chan, H. Yu, H. Jiang, *Nat. Commun.* **2014**, *5*, 3140.

[6] S. Xu, Y. Zhang, J. Cho, J. Lee, X. Huang, L. Jia, J. A. Fan, Y. Su, J. Su, H. Zhang, H. Cheng, B. Lu, C. Yu, C. Chuang, T. I. Kim, T. Song, K. Shigeta, S. Kang, C. Dagdeviren, I. Petrov, P. V. Braun, Y. Huang, U. Paik, J. A. Rogers, *Nat. Commun.* **2013**, *4*, 1543.

[7] D.-H. Kim, N. Lu, R. Ma, Y.-S. Kim, R.-H. Kim, S. Wang, J. Wu, S. M. Won, H. Tao, A. Islam, K. J. Yu, T.-I. Kim, R. Chowdhury, M. Ying, L. Xu, M. Li, H.-J. Chung, H. Keum, M. McCormick, P. Liu, Y.-W. Zhang, F. G. Omenetto, Y. Huang, T. Coleman, J. A. Rogers, *Science* **2011**, *333*, 838.

[8] D. H. Kim, Z. Liu, Y. S. Kim, J. Wu, J. Song, H. S. Kim, Y. Huang, K. C. Hwang, Y. Zhang, J. A. Rogers, *Small* **2009**, *5*, 2841.

[9] Y. Morikawa, S. Yamagiwa, H. Sawahata, R. Numano, K. Koida, M. Ishida, T. Kawano, *Adv. Healthcare Mater.* **2018**, *7*, 1701100.

[10] T. C. Shyu, P. F. Damasceno, P. M. Dodd, A. Lamoureux, L. Xu, M. Shlian, M. Shtein, S. C. Glotzer, N. A. Kotov, *Nat. Mater.* **2015**, *14*, 785.

[11] Z. Liu, X. Wang, D. Qi, C. Xu, J. Yu, Y. Liu, Y. Jiang, B. Liedberg, X. Chen, *Adv. Mater.* **2017**, *29*, 1603382.

[12] M. Drack, I. Graz, T. Sekitani, T. Someya, M. Kaltenbrunner, S. Bauer, *Adv. Mater.* **2015**, *27*, 34.

[13] R. Nur, N. M., Z. Jiang, Md. O. G. Nayeem, T. Yokota, T. Someya, *Nano Lett.* **2018**, *18*, 5610.

[14] S. Park, S. W. Heo, W. Lee, D. Inoue, Z. Jiang, K. Yu, H. Jinno, D. Hashizume, M. Sekino, T. Yokota, K. Fukuda, K. Tajima, T. Someya, *Nature* **2018**, *561*, 516.

[15] D. J. Lipomi, *Adv. Mater.* **2016**, *28*, 4180.

[16] O. Akogwu, D. Kwabi, A. Munhutu, T. Tong, W. O. Soboyejo, *J. Appl. Phys.* **2010**, *108*, 123509.

[17] Z. H. Chen, R. Fang, W. Li, J. Guan, *Adv. Mater.* **2019**, *31*.

[18] D. McCoul, W. Hu, M. Gao, V. Mehta, Q. Pei, *Adv. Electron. Mater.* **2016**, *2*, 1500407.

[19] S. Park, K. Parida, P. S. Lee, *Adv. Energy Mater.* **2017**, *7*, 1701369.

[20] J. Rivnay, S. Inal, B. A. Collins, M. Sessolo, E. Stavrinidou, X. Strakosas, C. Tassone, D. M. Delongchamp, G. G. Malliaras, *Nat. Commun.* **2016**, *7*, 11287.

[21] C. Wan, K. Xiao, A. Angelin, M. Antonietti, X. Chen, *Adv. Intell. Syst.* **2019**, *1*, 1900073.

[22] J. C. Dias, D. M. Correia, C. M. Costa, C. Ribeiro, A. Maceiras, J. L. Vilas, G. Botelho, V. de Zea Bermudez, S. Lanceros-Mendez, *Electrochim. Acta* **2019**, *296*, 598.

[23] C. H. Yang, Z. G. Suo, *Nat. Rev. Mater.* **2018**, *3*, 125.

[24] S. Z. Bisri, S. Shimizu, M. Nakano, Y. Iwasa, *Adv. Mater.* **2017**, *29*, 1607054.

[25] J. Y. Sun, C. Keplinger, G. M. Whitesides, Z. Suo, *Adv. Mater.* **2014**, *26*, 7608.

[26] Z. Lei, Q. Wang, S. Sun, W. Zhu, P. Wu, *Adv. Mater.* **2017**, *29*.

[27] B. Ying, Q. Wu, J. Li, X. Liu, *Mater. Horiz.* **2020**, *7*, 477.

[28] Z. Lei, P. Wu, *Nat. Commun.* **2018**, *9*, 1134.

[29] C. H. Yang, B. Chen, J. J. Lu, J. H. Yang, J. Zhou, Y. M. Chen, Z. Suo, *Extreme Mech. Lett.* **2015**, *3*, 59.

[30] X. Pu, M. Liu, X. Chen, J. Sun, C. Du, Y. Zhang, J. Zhai, W. Hu, Z. L. Wang, *Sci. Adv.* **2017**, *3*, 1700015.

[31] K. Parida, V. Kumar, W. Jiangxin, V. Bhavanasi, R. Bendi, P. S. Lee, *Adv. Mater.* **2017**, *29*, 1702181.

[32] Y. Bai, Y. Chen, F. Xiang, J. Zhou, H. Wang, Z. Suo, *Appl. Phys. Lett.* **2014**, *105*, 151903.

[33] X. P. Morelle, W. R. Illeperuma, K. Tian, R. Bai, Z. Suo, J. J. Vlassak, *Adv. Mater.* **2018**, *30*, 1801541.

[34] Y. Ye, Y. Zhang, Y. Chen, X. Han, F. Jiang, *Adv. Funct. Mater.* **2020**, *30*, 2003430.

[35] L. Fang, J. Zhang, W. Wang, Y. Zhang, F. Chen, J. Zhou, F. Chen, R. Li, X. Zhou, Z. Xie, *ACS Appl. Mater. Interfaces* **2020**, *12*, 56393.

[36] H. Zhou, J. Lai, X. Jin, H. Liu, X. Li, W. Chen, A. Ma, Z. Xuechang, *Chem. Eng. J.* **2021**, *413*, 127544.

[37] Y. Lee, W. J. Song, Y. Jung, H. Yoo, M. Y. Kim, H. Y. Kim, J. Y. Sun, *Sci. Robot.* **2020**, *5*, eaaz5405.

[38] B. Yiming, Y. Han, Z. Han, X. Zhang, Y. Li, W. Lian, M. Zhang, J. Yin, T. Sun, Z. Wu, T. Li, J. Fu, Z. Jia, S. Qu, *Adv. Mater.* **2021**, *33*, 2006111.

[39] X. Qu, W. Niu, R. Wang, Z. Li, Y. Guo, X. Liu, J. Sun, *Mater. Horiz.* **2020**, *7*, 2994.

[40] H. J. Kim, B. Chen, Z. Suo, R. C. Hayward, *Science* **2020**, *367*, 773.

[41] L. Shi, T. Zhu, G. Gao, X. Zhang, W. Wei, W. Liu, S. Ding, *Nat. Commun.* **2018**, *9*, 2630.

[42] Y. M. Kim, H. C. Moon, *Adv. Funct. Mater.* **2019**, *30*, 1907290.

[43] D. M. Correia, L. C. F., P. M. Martins, C. García-Astrain, C. M. Costa, J. Reguera, S. Lanceros-Méndez, *Adv. Funct. Mater.* **2020**, *30*, 1909736.

[44] B. Chen, J. J. Lu, C. H. Yang, J. H. Yang, J. Zhou, Y. M. Chen, Z. Suo, *ACS Appl. Mater. Interfaces* **2014**, *6*, 7840.

[45] Y. Wang, Y. Chen, J. Gao, H. G. Yoon, L. Jin, M. Forsyth, T. J. Dingemans, L. A. Madsen, *Adv. Mater.* **2016**, *28*, 2571.

[46] Y. Ding, J. Zhang, L. Chang, X. Zhang, H. Liu, L. Jiang, *Adv. Mater.* **2017**, *29*, 1704253.

[47] E. Kamio, T. Yasui, Y. Iida, J. P. Gong, H. Matsuyama, *Adv. Mater.* **2017**, *29*, 1704118.

[48] Y. Ren, J. Guo, Z. Liu, Z. Sun, Y. Wu, L. Liu, Y. Feng, *Sci. Adv.* **2019**, *5*, eaax0648.

[49] Z. Lei, P. Wu, *Nat. Commun.* **2019**, *10*, 3429.

[50] Z. Cao, H. Liu, L. Jiang, *Mater. Horiz.* **2020**, *7*, 912.

[51] L. Chen, T. L. Sun, K. Cui, D. R. King, T. Kurokawa, S. Yoshiyuki, J. P. Gong, *J. Mater. Chem. A* **2019**, *7*, 17334.

[52] L. Shi, K. Jia, Y. Gao, H. Yang, Y. Ma, S. Lu, G. Gao, H. Bu, T. Lu, S. Ding, *Research* **2020**, 2020.

[53] C. Yang, T. Yin, Z. Suo, *J. Mech. Phys. Solids* **2019**, *131*, 43.

[54] C. Chen, Z. Wang, Z. Suo, *Extreme Mech. Lett.* **2017**, *10*, 50.

[55] J. Tang, J. Li, J. J. Vlassak, Z. Suo, *Soft Matter* **2016**, *12*, 1093.

[56] Q. Liu, G. Nian, C. Yang, S. Qu, Z. Suo, *Nat. Commun.* **2018**, *9*, 846.

[57] Y. Wang, K. Jia, C. Xiang, J. Yang, X. Yao, Z. Suo, *ACS Appl. Mater. Interfaces* **2019**, *11*, 40749.

[58] J. Yang, R. Bai, Z. Suo, *Adv. Mater.* **2018**, *30*, 180071.

[59] Y. Gao, J. Chen, X. Han, Y. Pan, P. Wang, T. Wang, T. Lu, *Adv. Funct. Mater.* **2020**, *30*, 2003207.

[60] A. Zimmerman, L. Bai, D. D. Ginty, *Science* **2014**, *346*, 950.

[61] J. C. Yang, J. Mun, S. Y. Kwon, S. Park, Z. Bao, S. Park, *Adv. Mater.* **2019**, *31*, 1904765.

[62] T. Someya, M. Amagai, *Nat. Biotechnol.* **2019**, *37*, 382.

[63] T. R. Ray, J. Choi, A. J. Bandodkar, S. Krishnan, P. Gutruf, L. Tian, R. Ghaffari, J. A. Rogers, *Chem. Rev.* **2019**, *119*, 5461.